Journal of Power Sources 196 (2011) 5520–5525

Contents lists available at ScienceDirect

Journal of Power Sources

journal homepage: www.elsevier.com/locate/jpowsour

Free vibration analysis of a polymer electrolyte membrane fuel cell

H.E.U. Ahmed [a,b], R. Banan [a,b], J.W. Zu [a], A. Bazylak [b,*]

[a] Vibration and Computational Dynamics Laboratory, Dept. of Mechanical & Industrial Engineering, University of Toronto, 5 King's College Road, Toronto, ON, Canada M5S 3G8
[b] Microscale Energy Systems Transport Phenomena Laboratory, Dept. of Mechanical & Industrial Engineering, University of Toronto, 5 King's College Road, Toronto, ON, Canada M5S 3G8

ARTICLE INFO

Article history:
Received 2 August 2010
Received in revised form 6 October 2010
Accepted 7 October 2010
Available online 4 March 2011

Keywords:
Free vibrations
Polymer electrolyte membrane fuel cell
PEMFC
Natural frequency
Mode shapes
Composite layers

ABSTRACT

A free vibration analysis of a polymer electrolyte membrane fuel cell (PEMFC) is performed by modelling the PEMFC as a 20 cm × 20 cm composite plate structure. The membrane, gas diffusion electrodes, and bi-polar plates are modelled as composite material plies. Energy equations are derived based on Mindlin's plate theory, and natural frequencies and mode shapes of the PEMFC are calculated using finite element modelling. A parametric study is conducted to investigate how the natural frequency varies as a function of thickness, Young's modulus, and density for each component layer. It is observed that increasing the thickness of the bi-polar plates has the most significant effect on the lowest natural frequency, with a 25% increase in thickness resulting in a 17% increase in the natural frequency. The mode shapes of the PEMFC provide insight into the maximum displacement exhibited as well as the stresses experienced by the single cell under vibration conditions that should be considered for transportation and stationary applications. This work provides insight into how the natural frequencies of the PEMFC should be tuned to avoid high amplitude oscillations by modifying the material and geometric properties of individual components.

1. Introduction

Polymer electrolyte membrane fuel cells (PEMFCs) may be subject to vibrations under dynamic situations found in transportation applications as well as stationary applications near heavy traffic and rail transport. Passenger vehicles generally experience vibrations in the range of 8–16 Hz due to the unevenness of the road and the oscillation of the axel and wheel with the suspension system [1]. PEMFCs may be employed to power auxiliary devices in semi-trailers, which typically experience vibrations in the range of 0.9–5.8 Hz during highway driving conditions [2]. Buildings near busy roads are also subject to vibrations due to nearby traffic, which cause vibrations between 5 and 25 Hz [3]. When placed in applications such as these, the PEMFC may vibrate at an excitation frequency within the band of its natural frequencies and cause the PEMFC to vibrate in resonance with high amplitude. Therefore, it is critical to identify the natural frequencies that a PEMFC may experience in the context of the excitation frequencies expected in these applications. Vibrating at resonance frequency can lead to the initiation and acceleration of defect formation, which may ultimately result in operational failure. Vibrations may exacerbate defects such as pinholes, cracks, and delamination, which can result in fuel crossover, performance degradation, and reduced durability [4,5]. Vibration characteristics are required to understand the vibration behaviour of PEMFC components such as the membrane, catalyst layer, gas diffusion layers, and bi-polar plates.

Vibration tests on PEMFC stacks and mechanical non-linear behaviour modelling with neural networks and finite element modelling has been reported by several authors [6–13]. Rouss et al. [7] test a fuel cell stack under vibrations to simulate the operational conditions of an aircraft. They characterize the mechanical behaviour of the stack by determining the natural frequencies, and they find that the PEMFC behaves as a multi-body non-linear system. Each component of the fuel cell exhibits distinct frequency responses, in contrast to behaving like a rigid body. In a separate work, the authors develop a three-dimensional, multi-input and multi-output artificial neural network (ANN) model based on experimental findings from PEMFC vibration tests [8]. They propose a fuel cell neural network model, which can be used for monitoring purposes to detect abnormalities in the mechanical behaviour of a similar fuel cell stack placed under vibrating conditions.

The mechanical non-linear response of a PEMFC is characterized using acceleration data from vibration experiments by Rouss et al. [10]. They place accelerometers on the bi-polar plate with and without structural supports and find similarities between the results from a simple single degree of freedom (SDOF) system and from a complex multi-physics system based on a library of non-linear signatures. From temporal signals measured with one-dimensional and three-dimensional accelerometers, they find that the PEMFC

* Corresponding author. Tel.: +1 416 946 5031; fax: +1 416 978 7753.
E-mail address: abazylak@mie.utoronto.ca (A. Bazylak).

0378-7753/$ – see front matter © 2011 Elsevier B.V. All rights reserved.
doi:10.1016/j.jpowsour.2010.10.112

Nomenclature

A	cross-section area
a_i	coefficients of mode shape
D_b	the material property matrix for bending
D_s	the material property matrix for shear
D_{ij}	the coefficients of the bending and shear stiffness matrices
E_k	modulus of elasticity of the respective layer
h	thickness of the PEMFC
L	length of the PEMFC
$[K]$	assembled stiffness matrix
K^e	element stiffness matrix
$[M]$	assembled mass matrix
M^e	element mass matrix
n	the number of nodes per element
nc	the number of component layers
N_i	the shape functions
t	time variable
T	the kinetic energy
t_k	thickness of the respective layer
U	the strain energy
V	the volume of the PEMFC
w	displacement in the thickness direction
$\{w\}$	displacement vectors
$\{\ddot{w}\}$	acceleration vectors
x	longitudinal-direction of the PEMFC
y	width-direction of the PEMFC
z	thickness-direction of the PEMFC
σ_b	the bending stress tensor
σ_s	the shear stress tensor
ε_b	the bending strain tensor
ε_s	the shear strain tensor
θ_x	rotation about x-axis
θ_y	rotation about y-axis
ρ_k	density of the respective layer
α	shear correction factor
λ	Eigen value
ω_n	natural frequency
ν_k	Poisson's ratio of the respective layer
ξ,η	local coordinates

exhibits dry friction behaviour, which they attribute to the contact between the bi-polar plates and tie rods. To investigate the dynamic behaviour of a non-linear mechanical system, Rouss and Charon [11] measure the response of a non-linear mechanical system subjected to random, shock, and swept sine excitations on a vibrating platform. They employ these results to validate and train their numerical model.

Rajalakshmi et al. [6] subject a PEMFC stack to vibrations, which include random and swept-sine excitations on a vibrating platform in three axes. Although changes to the mechanical integrity of the stack are not detected, they find a compression force release at the bolts. Ozgur [14] performs modal analysis with experimental vibration investigations on an automotive fuel cell stack module in order to design a mounting bracket. They employ an electro-dynamic shaker test apparatus to identify the appropriate mounting system under resonance frequency considerations.

Betournay et al. [12] experimentally investigate the effects of mining conditions on the performance of a PEMFC. They determine the effects of shocks and vibrations on the performance of PEMFC and the effects of mineral and diesel particulate matter on the physical reliability/integrity of the fuel cell stack. They also evaluate the physical reliability/integrity of the fuel cell stack when mounted over the rear wheel of a mine loader chassis, which applied shocks and vibrations to the fuel cell.

Privette et al. [15] conduct vibration studies to qualify a PEMFC against US military vibration and shock standards. PEMFC stack testing has been recently studied in the framework of a European Union harmonized fuel cell testing protocol [16], which is comprised of 55 European partners. Fuel cell testing protocols include the application of vibrations and shocks with 6 degrees of freedom at a frequency of up to 250 Hz.

To the authors' best knowledge, free vibration analysis using the finite element method has yet to be performed. In this work, the finite element model for simulating the PEMFC as a composite material is presented. Free vibrations are simulated for the composite, which consists of a membrane, gas diffusion electrodes (GDEs), and bi-polar plates. A parametric study is conducted to investigate how the natural frequency varies as a function of thickness, Young's modulus, and density for each component layer.

2. Finite element formulations

In this work, the finite element method is employed for the free vibration analysis of a PEMFC, with degrees of freedom for the transverse displacement and rotation with respect to the x- and y-directions. The PEMFC is modelled as a symmetrically laminated composite plate, composed of a membrane, gas diffusion electrodes (GDEs) and bi-polar plates, which are considered plies of the composite plate. The GDE is the gas diffusion layer combined with the catalyst layer. The bi-polar plate is modelled as a solid graphite layer, without flow fields. Since the PEMFC is modelled as a composite, interfaces between the layers are not considered here. For the free vibration analysis of a PEMFC, clamped boundary conditions are applied to all edges.

Isoparametric shape functions are employed for the plate element formulations. The generalized transverse displacement and rotations are interpolated as follows [17]:

$$w = \sum_{i=1}^{n} N_i(\xi, \eta) W_i \tag{1a}$$

$$\theta_x = \sum_{i=1}^{n} N_i(\xi, \eta) \theta_{x_i} \tag{1b}$$

$$\theta_y = \sum_{i=1}^{n} N_i(\xi, \eta) \theta_{y_i} \tag{1c}$$

where n is the number of nodes per element. $N_i(\xi,\eta)$ represents the shape functions of a bilinear four-node quadrilateral element in natural coordinates, based on a local coordinate system with independent variablesξ and η. w, θ_x and θ_y are the transverse displacements in the z-direction, and rotations of the normal to the mid-plane with respect to the x and y-direction, respectively. w_i, θ_{x_i}, and θ_{y_i} are the nodal transverse displacements in the z-direction and the nodal rotation with respect to x-direction and y-direction, respectively. The shape functions of a 4-node bilinear quadrilateral element, which are used in the strain–displacement relation of the energy formulation section, are as follows:

$$N_1(\xi, \eta) = \frac{1}{4}(1-\xi)(1-\eta) \tag{2a}$$

$$N_2(\xi, \eta) = \frac{1}{4}(1+\xi)(1-\eta) \tag{2b}$$

$$N_3(\xi, \eta) = \frac{1}{4}(1+\xi)(1+\eta) \tag{2c}$$

$$N_4(\xi, \eta) = \frac{1}{4}(1-\xi)(1+\eta) \tag{2d}$$

Mindlin's plate theory [18] is utilized for the energy formulation, which incorporates the transverse shear deformation. The fundamental assumption is that the plate cross-section remains plane and normal to the deformed longitudinal axis before bending, but does not necessarily remain normal to the deformed middle plane of the plate after bending. Taking into account the basic assumptions of Mindlin's plate theory for a PEMFC, the strain energy is written as:

$$U = \frac{1}{2}\int_v \sigma_b \varepsilon_b \mathrm{d}V + \frac{\alpha}{2}\int_v \sigma_s \varepsilon_s \mathrm{d}V \tag{3}$$

where σ_b denotes the bending stress field tensor, ε_b denotes the bending strain field tensor, σ_s denotes the transverse shear stress field tensor, and ε_s denotes the transverse shear strain field tensor. V is the volume of the plate, and α is the shear correction factor. Subscripts b and s denote bending and shear, respectively.

The linear elastic stress–strain relations in bending are defined for an isotropic material as the following:

$$\sigma_b = D_b \varepsilon_b \tag{4}$$

The material property matrix for bending of a symmetric laminated composite plate is given by [19]:

$$D_b = \begin{bmatrix} D_{11} & D_{12} & D_{16} \\ D_{12} & D_{22} & D_{26} \\ D_{16} & D_{26} & D_{66} \end{bmatrix} \tag{5}$$

where

$$D_{11} = \sum_{k=1}^{nc} \frac{E_k}{1-\upsilon_k^2}\left(t_k Z_k^2 + \frac{t_k^3}{12}\right) \tag{6a}$$

$$D_{12} = \sum_{k=1}^{nc} \frac{\upsilon_k E_k}{1-\upsilon_k^2}\left(t_k Z_k^2 + \frac{t_k^3}{12}\right) \tag{6b}$$

$$D_{22} = D_{11} \tag{6c}$$

$$D_{16} = D_{26} = 0 \tag{6d}$$

$$D_{66} = \sum_{k=1}^{nc} \frac{\upsilon_k E_k}{2(1-\upsilon_k^2)}\left(t_k Z_k^2 + \frac{t_k^3}{12}\right) \tag{6e}$$

E_k denotes Young's modulus, υ_k denotes Poisson's ratio, t_k denotes the thickness of the component layers, and the subscript k denotes the respective component layer.

The linear elastic stress–strain relationship for shear is defined for an isotropic material as:

$$\sigma_s = D_s \varepsilon_s \tag{7}$$

The material property matrix for the shear of a symmetric laminated composite plate is given by:

$$D_s = \begin{bmatrix} D_{77} & 0 \\ 0 & D_{88} \end{bmatrix} \tag{8}$$

where

$$D_{77} = D_{88} = \sum_{k=1}^{nc} \frac{E_k}{1-\upsilon_k} t_k \tag{9}$$

The maximum strain energy of the plate is written as:

$$U = \frac{1}{2}\int_v [\varepsilon_b]^T [D_b][\varepsilon_b]\mathrm{d}V + \frac{\alpha}{2}\int_v [\varepsilon_s]^T [D_s][\varepsilon_s]\mathrm{d}V \tag{10}$$

The kinetic energy for a plate is given by:

$$T = \frac{1}{2}\int \rho\left[h\dot{w}^2 + \frac{h^3}{12}\dot{\theta}_x^2 + \frac{h^3}{12}\dot{\theta}_y^2\right]\mathrm{d}A \tag{11}$$

where ρ is the density, h is the thickness of the plate, and A the cross-sectional area.

The total functional energy in the absence of work from external forces is expressed as:

$$\Pi = U - T \tag{12}$$

By imposing the stationary condition ($\partial\Pi/\partial w = 0$) to Eq. (12), the element stiffness matrix, K^e, and mass matrix, M^e, are calculated as follows:

$$K^e = \int_A B_b^T D_{bk} B_b \mathrm{d}A + \alpha\int_A B_S^T D_{sk} B_s \mathrm{d}A \tag{13}$$

$$M^e = \int_A N^T\left(\sum_{k=1}^{nc}\rho_k \begin{bmatrix} t_k & 0 & 0 \\ 0 & t_k^3/12 & 0 \\ 0 & 0 & t_k^3/12 \end{bmatrix}\right) N\mathrm{d}A \tag{14}$$

By substituting the local coordinates in the element area, the element stiffness and mass matrices are computed with the Gauss–Legendre quadrature numerical integration as follows [17]:

$$K^e = \int_{-1}^{1}\int_{-1}^{1} B_b^T D_b B_b [J]\mathrm{d}\xi\mathrm{d}\eta + \alpha\int_{-1}^{1}\int_{-1}^{1} B_S^T D_s B_s [J]\mathrm{d}\xi\mathrm{d}\eta \tag{15}$$

$$M^e = \int_{-1}^{1}\int_{-1}^{1} N^T\left(\sum_{k=1}^{nc}\rho_k \begin{bmatrix} tk & 0 & 0 \\ 0 & t_k^3/12 & 0 \\ 0 & 0 & t_k^3/12 \end{bmatrix}\right) N\left|J\right|\mathrm{d}\xi\mathrm{d}\eta \tag{16}$$

where $\left|J\right|$ is the determinant of the Jacobian matrix. After calculating element stiffness and mass matrices using a numerical program written in Matlab [20], the matrices are assembled together to form the overall stiffness and mass matrices for a complete single PEMFC. These assembled stiffness and mass matrices are used in the equation of motion, which is discussed in the section below.

3. Solution

The equation of motion for a free vibration of a structure is written as:

$$[M]\{\ddot{w}\} + [K]\{w\} = 0 \tag{17}$$

where $[M]$, $[K]$, $\{w\}$ are the mass matrix, stiffness matrix, and displacement matrices, respectively. To find the natural motion of a structure, the form of response or solution is assumed as:

$$\{w(t)\} = \{Z\}\mathrm{e}^{i\omega t} \tag{18}$$

where $\{Z\}$ is the mode shape (Eigen vector), and ω is the natural frequency. The general solution is a linear combination of each mode:

$$\{w(t)\} = a_1\{Z_1\}\mathrm{e}^{i\omega_1 t} + a_2\{Z_2\}\mathrm{e}^{i\omega_2 t} + a_3\{Z_3\}\mathrm{e}^{i\omega_3 t} + \cdots \tag{19}$$

where each constant (a_i) can be evaluated from the initial conditions. Substituting Eq. (18) into Eq. (17) yields:

$$([K] - \omega^2[M])\{Z\}\mathrm{e}^{i\omega t} = 0 \tag{20}$$

The above equation has a nontrivial solution if $\left|[K] - \omega^2[M]\right|$ becomes singular. In other words, there exists n number of solutions, $(\omega_1^2, \omega_2^2, \ldots \omega_n^2)$, which satisfy the following equation:

$$\left|[K] - \lambda[M]\right|\{Z\} = \{0\} \tag{21}$$

where $\lambda = \omega^2$ is the Eigen value of the system.

From a grid sensitivity study, a 10×10 element mesh is found to provide reasonable convergence and is utilized for all simulations presented in this work. The lowest three natural frequencies are calculated and presented in Table 1. Based on this convergence study, doubling the mesh density would only result in a 0.2% difference in the calculated first natural frequencies. Therefore, the mesh density employed in this work is sufficient. A schematic of the discretized PEMFC is shown in Fig. 1.

Table 1
Comparison of natural frequencies (Hz) of a PEMFC for different element meshes.

Mode number	5 × 5-mesh	6 × 6-mesh	8 × 8-mesh	10 × 10-mesh	12 × 12-mesh	15 × 15-mesh
First mode	2328.80	2318.10	2310.70	2308.54	2307.73	2307.36
Second mode	4430.50	4386.80	4356.80	4450.88	4340.08	4344.08
Third mode	6064.00	6009.20	5966.70	5965.83	5956.67	5954.95

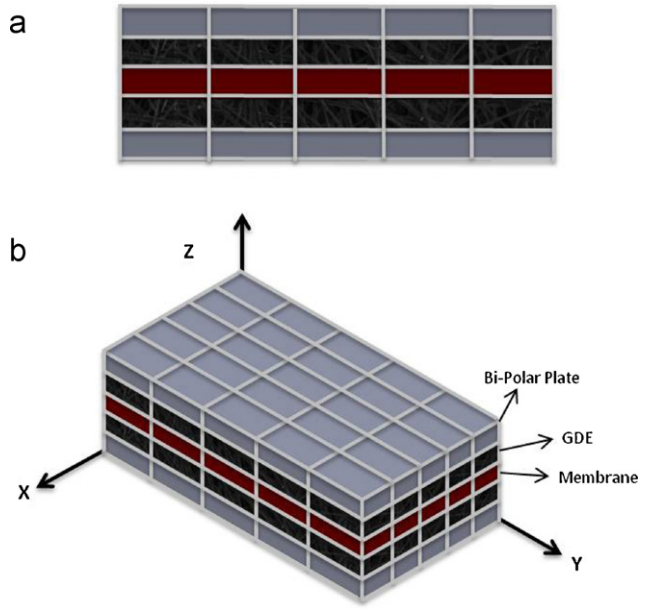

Fig. 1. A schematic of the discretized mesh for the PEMFC (a) top view and (b) three-dimensional view.

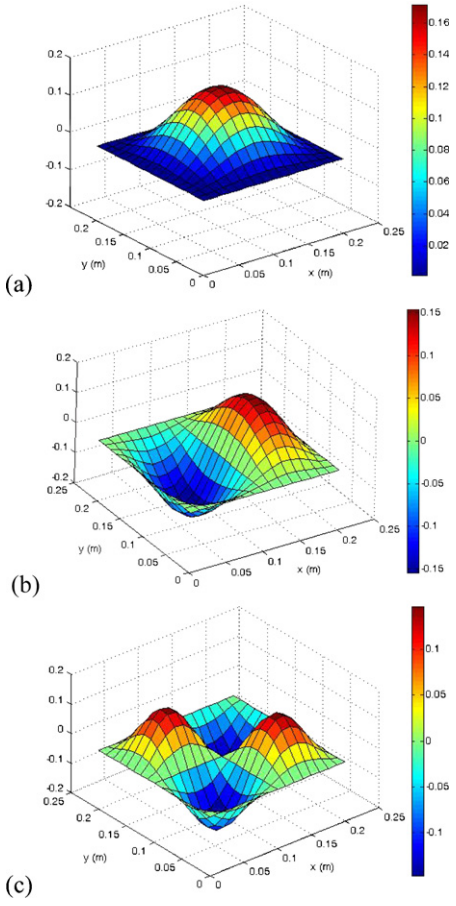

Fig. 2. Normal mode shapes for a PEMFC considered as a Mindlin's composite plate (a) first mode, (b) second mode, and (c) third mode.

4. Parametric study

A parametric study is performed to investigate the mechanical and geometrical property effects on the vibration characteristics of a PEMFC. The thickness, Young's modulus, and density for each component layer are increased independently in increments of 5% to a maximum of 25% of the base case value, and the impact on the natural frequency of the first mode is determined. Mechanical and geometrical properties for the base case simulation are obtained from [21] and are listed in Table 2.

The mode shapes for this base case are shown in Fig. 2, which provides insight into the maximum displacement exhibited as well as the stresses experienced by the material.

4.1. Influence of material thickness

Fig. 3 illustrates the impact of independently increasing the thickness of the PEMFC components on the lowest natural frequency. 5% increments of the thickness in the bi-polar plate, GDE, and membrane result in increases of thickness on the order of 10^{-1}, 10^{-2} and 10^{-3}, respectively. The dominating effect of the bipolar plate thickness is exacerbated by the t_k^3 term in the material property matrix (Eqs. (6a–e), (9) and (14)). Therefore, increasing the thickness of the GDEs and membrane result in negligible changes to the stiffness and mass matrices and negligible increases to the lowest natural frequency (less than 1%). However, increases to the thickness of the bi-polar plates result in a significant linear increase in the lowest natural frequency, with an increase of approximately 17% when the thickness of the plates increases by 25%.

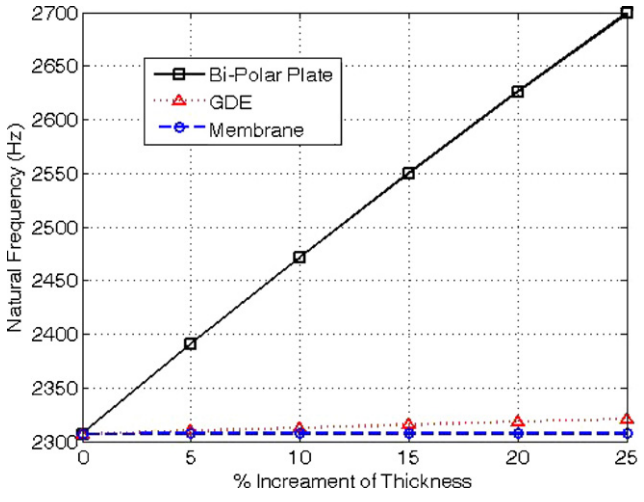

Fig. 3. Effect of independently varying component thickness on the first natural frequency.

Table 2
Mechanical and physical properties of the PEMFC for the base case simulation [21].

	Young's modulus (GPa)	Poisson's ratio	Density (kg m^{-3})	Thickness (mm)	Length (mm)	Width (mm)
Bi-polar plate	10	0.25	1800	12.8	200	200
GDE	10	0.25	400	0.28	200	200
Membrane	0.197	0.25	2000	0.05	200	200

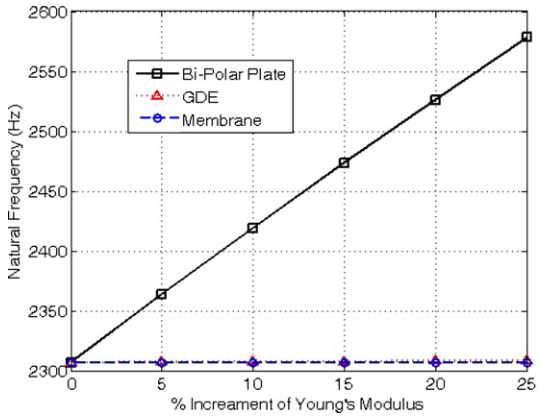

Fig. 4. Effect of independently varying Young's modulus on the first natural frequency.

4.2. Influence of Young's modulus

The effect of independently increasing the Young's modulus for the bi-polar plates, GDEs and membrane on the lowest natural frequency is shown in Fig. 4. Variations in the Young's modulus of the bi-polar plates and the GDEs both have the same impact on the natural frequency of the material, with increases resulting in a linear increase to the natural frequency. With a 25% increase in the Young's modulus, the natural frequency increases by approximately 12%. On the other hand, the natural frequency is not affected by increasing the Young's modulus of the membrane since its thickness is significantly smaller than the other two layers.

4.3. Influence of material density

Fig. 5 illustrates the effect of independently increasing the density of the bi-polar plates, GDEs and membrane on the lowest natural frequency. The combination of the order of magnitude of density and thickness will be the determinant factors in this behaviour. Since the densities of the bi-polar plate and membrane are almost 4.5 times greater than the GDE, and the thickness of the GDE and membrane are much less than the thickness of the bipolar plate, increasing the density for the GDEs and membrane do not result in any significant changes to the lowest natural frequency. On the other hand, increasing the density of the bi-polar plates results in a strong linear dependence of the lowest natural frequency. Increasing the density by 25% results in a decrease of the lowest natural frequency by approximately 11%. The effects of this parametric study have also been performed on the 2nd and 3rd modes, which resulted in similar trends.

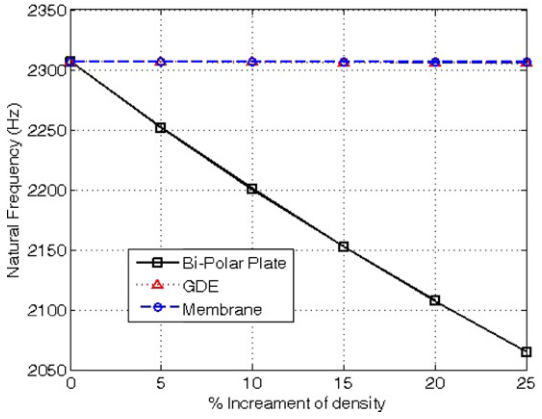

Fig. 5. Effect of independently varying the component density on first natural frequency.

5. Conclusions

A three-dimensional finite element model for the PEMFC modelled as a laminated composite structure using Mindlin's plate theory is presented. The model is employed to characterize the vibration behaviour of the PEMFC modelled with the membrane, GDEs, and bi-polar plates considered as composite material plies. A base case simulation is performed, and the mode shapes for the first three modes are presented.

A parametric study is performed to investigate the effect of independently increasing the thickness, Young's modulus, and density of the bi-polar plates, GDEs and membrane on the lowest natural frequency. It is found that increases in the GDE and membrane thickness have little effect, while increases in the bi-polar plate thickness has the most dominant effect on the natural frequency of the entire study. To a lesser degree, increasing the Young's modulus of the bi-polar plates and GDEs and increasing the density of the bi-polar plate also have a significant effect on the lowest natural frequency. Increasing the Young's modulus of the bi-polar plates and GDEs result in a linear increase in the natural frequency, while increasing the density of the bi-polar plates results in a linear decrease in the natural frequency. These results provide insight into how the natural frequencies of the PEMFC may be tuned to avoid high amplitude vibrations by modifying the material and geometric properties of individual components.

The magnitude of the natural frequencies for this single PEMFC have been found to be out of the range of frequencies (1–25 Hz) encountered in common transportation and stationary applications [1–3]. Future work includes the representation of the PEMFC as separate layers pressed together, so that the interfacial effects between layers can be investigated. In this investigation, one single cell is investigated to provide insight into the dominance of the component layers. However, practical applications require fuel cell stacks to provide realistic power levels. Since free vibrations that coincide with the natural frequency will result in high amplitude resonance vibrations, further investigations are required to determine whether the fuel cell stack will experience failure modes due to these application-based vibrations. Furthermore, in these practical applications, fuel cells will be assembled under compression, so our future investigations will include multiple PEMFC cells assembled together to form a fuel cell stack, which will provide the proper context in which to investigate vibration-resistant material properties and stack geometry. Furthermore, the absence of flow fields in the bi-polar plate structure may also affect the results presented here; therefore the flow field will also be included in our future work.

Acknowledgements

The Natural Sciences and Engineering Research Council of Canada (NSERC), Bullitt Foundation, and University of Toronto are gratefully acknowledged for their financial support. The authors would like to extend special thanks to Jongmin Lee and Zachary Fishman for their assistance with Fig. 1.

References

[1] G.R. Watts, V.V. Krylov, Applied Acoustics 59 (2000) 221–236.
[2] R. Hassan, K. McManus, Journal of Low Frequency Noise Vibration and Active Control 21 (2) (2002) 65–76.
[3] O. Hunaidi, Construction Technology Update 39 (2000) 1–6.
[4] Y. Li, D.A. Dillard, S.W. Case, M.W. Ellis, Y. Lai, C.S. Gittleman, D.P. Miller, Journal of Power Sources 194 (2009) 873–879.
[5] S. Kim, M.M. Mench, Journal of Power Sources 174 (2007) 206–220.
[6] N. Rajalakshmi, S. Pandien, K.S. Dhathathreyan, International Journal of Hydrogen Energy 34 (2009) 3833–3837.
[7] V. Rouss, P. Lesage, S. Begot, D. Candusso, W. Charon, F. Harel, X. Francois, V. Selinger, C. Schilo, S. Yde, International Journal of Hydrogen Energy 33 (2008) 6755–6765.
[8] V. Rouss, D. Candusso, W. Charon, International Journal of Hydrogen Energy 33 (2008) 6281–6288.
[9] V. Rouss, W. Charon, A. Desflots, International Journal of Hydrogen Energy 34 (2009) 2377–2386.
[10] V. Rouss, W. Charon, G. Cirrincione, Mechanical Systems and Signal Processing 23 (2009) 1145–1159.
[11] V. Rouss, W. Charon, Journal of Power Sources 175 (2008) 1–17.
[12] M.C. Betournay, G. Bonnel, E. Edwardson, D. Paktunc, A. Kaujman, A.T. Lomma, Journal of Power Sources 134 (2004) 80–87.
[13] D. Schmal, C.E. Kluiters, I.P. Barendregt, Journal of Power Sources 61 (1996) 255–257.
[14] K. Ozgur, International ANSYS Conference Proceedings, 2004, Ch. 1–11.
[15] R.M. Privette, T.A. Flynn, M.A. Perna, R. Holland, S. Rahmani, C. Woodburn, S.W. Scoles, R.C. Watson, International Fuel Cell Conference Proceedings, 1999, pp. 1–5.
[16] R. Bove, T. Malkow, A. Saturnio, G. Tsotridis, Journal of Power Sources 180 (2008) 452–460.
[17] D.W. Pepper, J.C. Heinrich, The Finite Element Method: Basic Concepts and the Applications, second ed., Taylor & Francis, New York, NY, 2006, Ch. 4–6.
[18] K.M. Liew, Journal of Sound and Vibration 198 (3) (1996) 343–360.
[19] J.M. Bertholet, Composite Materials: Mechanical Behaviour and Structural Analysis, Springer, New York, NY, 1999, Ch. 13–22.
[20] Y.W. Know, H. Bang, The Finite Element Method Using MATLAB, CRC Press, Boca Raton, FL, 2000, Ch. 6–10.
[21] D. Bograchev, M. Gueguen, J.C. Grandidier, S. Martemianov, International Journal of Hydrogen Energy 33 (2008) 5703–5717.